Destabilizing effect of plane Couette flow

T. Tatsuno and Z. Yoshida
Graduate School of Frontier Sciences, The University of Tokyo, Tokyo 113-0033, Japan

S. M. Mahajan
Institute for Fusion Studies, The University of Texas at Austin, Austin, Texas 78712

(Received 13 January 2003; accepted 14 March 2003)

In contrast to its well-known stabilization of the low-frequency plasma motions, a shear flow may equally effectively destabilize a class of plasma modes. The latter quality of the flow is illustrated by studying an incompressible ideal plasma with a simple velocity profile (Couette flow in a finite interval); it is found that interchange modes are driven more unstable through their interactions with the shear flow. In the presence of the flow shear, the growth rate of the perturbation increases due to the coupling of the Alfvén wave with a Rayleigh–Taylor-type instability drive. Marginally stable modes in the flowless equilibrium achieve their maximum growth rate when the maximum flow velocity becomes comparable to the Alfvén velocity. At larger shear flow velocities, however, the stabilizing ''stretching'' effect becomes dominant and the instability is quenched.
 [DOI: 10.1063/1.1573211]

I. INTRODUCTION

Shear flow induced suppression of turbulence is argued to come about through the scale-reduction of the fluctuations caused by the stretching of modes in a shear flow. This argument for stability, however, ignores the fact the available free energy associated with a shear flow may be a potent source for the destabilization of some other class of fluctuations. The Kelvin–Helmholtz (KH) instability, for instance, is a well-known example of an instability[1] that feeds on the ambient flow-energy. The effect of shear flows on plasma stability is quite complicated,[2–4] and has to be handled case by case.

As a general rule, the initial turning on of the shear flow is destabilizing. As the strength of the shear flow mounts, i.e., the maximum velocity crosses a certain critical value, the role is reversed and the flow exerts a stabilizing influence leading to complete stability eventually (as far as exponential instabilities are concerned). For a perturbation to grow preserving the mode structure, it must stay stationary against the stretching effect of the ambient flow. When local flow velocity considerably exceeds any possible phase velocity of a wave in the medium, no mode can withstand the flow, and the flow destroys the entire spectrum accessible to the flowless system. This explains the process of shear-flow stabilization within the framework of linear theory. If the shear flow is weak so that it merely affects but does not overwhelm the mode, an appropriate distribution of fluctuations could absorb net positive energy from the ambient flow causing an instability or enhancing the instability growth rate.

In this paper, we investigate the destabilizing/stabilizing effect of a shear flow for a simple model of an incompressible magnetized ideal plasma. For electrostatic mode devoid of Alfvén perturbations ($k_\parallel = 0$; $k_\parallel$ is the wave number parallel to the ambient magnetic field) one expects a decrease in the growth rate because the mode is easily stretched by advection. The situation is more complicated in electromagnetic modes with finite $k_\parallel$. As long as the local flow velocity is everywhere smaller than the Alfvén velocity, the Alfvén wave may propagate backwards and set up a standing mode. The stretching effect, however, will overcome the ability of the fluctuations to establish eigenmodes when the local speed of the flow is sufficiently large.

In Sec. II, we formulate the model. We review the static equilibrium in Sec. III followed by general remarks on the spectra of plane Couette flow system in Sec. IV. Detailed calculations of the unstable eigenvalue are given in Secs. V–VII: Section V is devoted to a perturbative treatment for small flow shear. We show that the growth rate of unstable eigenmodes increases with the increasing strength of the flow shear. The second order (with respect to flow shear) correction of the eigenvalue contains destabilizing term proportional to $k_\parallel^2$, which suggests that the destabilizing effect of shear flow is caused by the Alfvén wave. A variational method (Ritz approximation) is used to evaluate the approximate dispersion relation in Sec. VI. We show that the growth rate reaches its maximum (with respect to flow shear) when the maximum local flow velocity is comparable to the phase velocity of the Alfvén wave. Numerical analyses of the eigenvalue problem are given in Sec. VII. In Sec. VIII, we discuss the physical mechanism for destabilization, and summarize our results.

II. MODEL

We consider a one-dimensional slab plasma in a finite domain $[-a,a]$ which obeys ideal incompressible magnetohydrodynamic (MHD) equations with ambient fields consisting of a Couette flow $\mathbf{V}_0=(0,V_y(x),0)$ and a straight homogeneous magnetic field $\mathbf{B}_0=(0,B_y,B_z)$. Representing the interchange (Rayleigh–Taylor) drive by an effective gravity g (constant) in the direction of ∇x (see Fig. 1), the linear dynamics of ideal incompressible plasma of variable density is governed by[14]

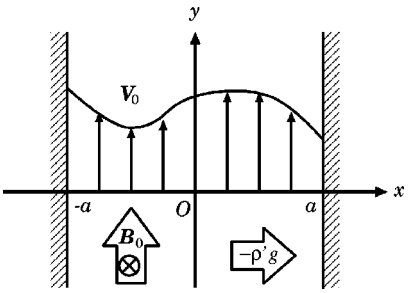

FIG. 1. Slab geometry with gravity.

$$(\partial_t + V_y\partial_y)\Delta\phi - V_y''\partial_y\phi = \frac{\mathbf{B}_0\cdot\nabla}{\mu_0\rho_0}\Delta\psi + \frac{g}{\rho_0}\partial_y\rho_1, \tag{1}$$

$$(\partial_t + V_y\partial_y)\rho_1 = -\rho_0'\partial_y\phi, \tag{2}$$

$$(\partial_t + V_y\partial_y)\psi = \mathbf{B}_0\cdot\nabla\phi, \tag{3}$$

where ρ_1, ϕ and ψ are, respectively, the mass density, the stream function ($\boldsymbol{v}=\nabla\phi\times\mathbf{e}_z$) and the flux function ($\mathbf{b}=\nabla\psi\times\mathbf{e}_z$) for the perturbed fields.[5] Subscript 0 denotes the equilibrium field, the prime the x-derivative, and $\Delta=\partial_x^2+\partial_y^2$ is the two-dimensional Laplacian operator. Note that the velocity field is chosen to be solenoidal ($\nabla\cdot\boldsymbol{v}=0$). The boundary conditions are $v_x(\pm a,y,t)=0$ and $b_x(\pm a,y,t)=0$, implying fixed conducting walls at $x=\pm a$.

Assuming $\mathbf{B}_0\cdot\nabla\neq 0$, we may combine (1)–(3) to obtain

$$(\partial_t + V_y\partial_y)\Delta(\partial_t + V_y\partial_y)\psi - V_y''\partial_y(\partial_t + V_y\partial_y)\psi = \frac{(\mathbf{B}_0\cdot\nabla)^2}{\mu_0\rho_0}\Delta\psi - \frac{\rho_0' g}{\rho_0}\partial_y^2\psi. \tag{4}$$

For the flowless equilibrium ($V_y=0$), the first term on the right-hand side expresses the stabilizing effect of the magnetic field line bending, while the second represents the destabilizing interchange drive for $\rho_0'<0$.

When $\mathbf{B}_0=\mathbf{0}$ and $\rho_0'>0$, the system reduces to the one studied in Ref. 6 showing a secular (algebraic) instability of vorticity fluctuation for a piece-wise linear velocity profile. The choice $\rho_0'=0$ and $\mathbf{B}_0\neq\mathbf{0}$ yields a set with a similar physical structure: the coupling of the shear flow effect (convection and excitation) with a wave of some description (plasma oscillation, gravity wave, or Alfvén wave). The only difference for the latter is the existence of the Laplacian operator on the right-hand side of (1).

Using the Alfvén velocity $v_A=B_0/\sqrt{\mu_0\rho_0}$ as the measure for the flow velocity and along with the following normalizations,

$$t=\frac{a}{v_A}\hat{t},\quad x=a\hat{x},\quad V_y=v_A\hat{V}_y,$$

$$\mathbf{B}_0=B_0\hat{\mathbf{B}},\quad g=\frac{v_A^2}{a}\hat{g},\quad L_\rho=a\hat{L}_\rho, \tag{5}$$

$$\psi=aB_0\hat{\psi},\quad \phi=av_A\hat{\phi},\quad \rho_1=\rho_0\hat{\rho},$$

where $L_\rho=-\rho_0/\rho_0'$ denotes the characteristic scale length of the density gradient (including signs), (1)–(3) take the dimensionless form (omitting $\hat{}$ to simplify the notation),

$$(\partial_t + V_y\partial_y)\Delta\phi - V_y''\partial_y\phi = \mathbf{B}\cdot\nabla\Delta\psi + g\partial_y\rho, \tag{6}$$

$$(\partial_t + V_y\partial_y)\rho = \frac{1}{L_\rho}\partial_y\phi, \tag{7}$$

$$(\partial_t + V_y\partial_y)\psi = \mathbf{B}\cdot\nabla\phi. \tag{8}$$

We note that the system (6)–(8) is equivalent to the linearized version of high-β reduced MHD equations describing tokamak plasmas[7] with the replacement $g=2/R_0$ (R_0 is the major radius of the toroidal device). The V_y'' term of (6) is the source of the KH instability of the neutral fluids;[8,9] in the following analysis limited to linear profiles of the shear flow ($V_y''=0$), the standard KH drive will not appear. We also assume that L_ρ is a finite constant and the Alfvén velocity is homogeneous. Although the model system is considerably simplified, it will capture essentials of the mechanism of interaction between fluctuations and the ambient shear flow.

III. INTERCHANGE MODE FOR STATIC PLASMA

It may be appropriate to start with a brief review of the flowless ($\mathbf{V}_0=\mathbf{0}$) limit. When $\mathbf{B}\cdot\nabla=0$, the system reduces to an equivalent neutral fluid model. With $\mathbf{B}\cdot\nabla\neq 0$, (4) reads

$$\partial_t^2\Delta\psi = (\mathbf{B}\cdot\nabla)^2\Delta\psi + G\partial_y^2\psi, \tag{9}$$

where $G:=g/L_\rho$ ($=-a^2\rho_0' g/v_A^2\rho_0$ in physical units) denotes the strength of the interchange (Rayleigh–Taylor) drive (G is a constant).

The transformation $\partial_t\to -i\omega$ and $\nabla\to i\mathbf{k}$, converts (9) to the ordinary differential equation (ODE),

$$\frac{d^2\psi}{dx^2} - k_y^2\left(1+\frac{G}{\omega^2-k_\parallel^2}\right)\psi = 0, \tag{10}$$

where $k_\parallel=\mathbf{k}\cdot\mathbf{B}/|\mathbf{B}|$ is the wave number parallel to the ambient magnetic field (both are constants). The stream function obeys the same ODE. For the eigenfunctions to satisfy the boundary conditions, we need

$$k_\parallel^2 - G < \omega^2. \tag{11}$$

Since $k_\parallel^2>0$, the Alfvén wave acts to stabilize interchange modes. If (11) is satisfied, we obtain even and odd eigenmodes,

$$\psi=\begin{cases}\cos(n\pi x/2) & \text{for } n\text{: odd},\\ \sin(n\pi x/2) & \text{for } n\text{: even},\end{cases} \tag{12}$$

respectively. The eigenmodes contain $n-1$ nodes (zeros in ψ). The dispersion relation is

$$\omega^2 = k_\parallel^2 - \frac{k_y^2 G}{k_y^2 + n^2\pi^2/4}, \tag{13}$$

showing that ω^2 decreases monotonically as $|k_y|$ increases. The bound of ω^2 is $k_\parallel^2$, which is the accumulation point of ω_n^2 as $n\to\infty$; i.e.,

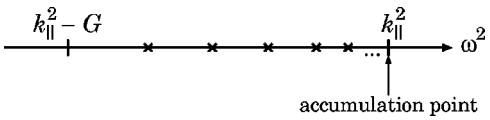

FIG. 2. Distribution of eigenvalues in ω^2 space.

$$k_\parallel^2 - G < \omega^2 < k_\parallel^2 . \tag{14}$$

The distribution of the eigenvalues is illustrated in Fig. 2, which represents a typical spectral structure of the discrete part of the shear Alfvén branch.[10]

If $k_\parallel^2$ is larger than the drive G, there is no instability even if $G>0$. The instability condition is given by

$$G > k_\parallel^2 \left(1 + \frac{\pi^2}{4k_y^2} \right). \tag{15}$$

IV. DISPERSION RELATION WITH FLOW

We now introduce a linear shear flow (σ is a real constant)

$$V_y(x) = \sigma x \tag{16}$$

for which the conventional KH instability is absent because $V_y'' = 0$ (see Sec. II). The modal transforms of (6)–(8) read as

$$\Omega \Delta \phi = -k_\parallel \Delta \psi - k_y g \rho, \tag{17}$$

$$\Omega \rho = -\frac{k_y}{L_\rho} \phi, \tag{18}$$

$$\Omega \psi = -k_\parallel \phi, \tag{19}$$

where $\Omega = \omega - k_y V_y(x)$ is the Doppler shifted local frequency. Simple algebra leads to the spectral ODE governing ψ,

$$\Omega \left(\frac{\mathrm{d}}{\mathrm{d}x} \left[(\Omega^2 - k_\parallel^2) \frac{\mathrm{d}\psi}{\mathrm{d}x} \right] - k_y^2 (\Omega^2 - k_\parallel^2 + G) \psi \right) = 0. \tag{20}$$

Here, we implicitly assumed $k_\parallel \neq 0$.

Equation (20) contains, in addition to other modes, the fully decoupled flow-induced continuous spectra $\Omega = 0$. For this continuous spectra,

$$\omega = k_y \sigma x_s \quad [\forall x_s \in (-1,1)], \tag{21}$$

and the corresponding eigenfunctions are determined by

$$\frac{\mathrm{d}}{\mathrm{d}x} \left[(\Omega^2 - k_\parallel^2) \frac{\mathrm{d}\psi}{\mathrm{d}x} \right] - k_y^2 (\Omega^2 - k_\parallel^2 + G) \psi = \delta(x - x_s). \tag{22}$$

As far as $\Omega^2 - k_\parallel^2 \neq 0$ is satisfied for all $x \in [-1,1]$, the eigenfunctions corresponding to the flow continuum ($\Omega = 0$) do not contain nonintegrable component in ψ. Due to the contribution of the δ-function on the right-hand side of (22), $\mathrm{d}\psi/\mathrm{d}x$ may contain finite jump, however, ψ does not diverge at $x = x_s$,

The standard branches of spectra are given by

$$\frac{\mathrm{d}}{\mathrm{d}x} \left[(\Omega^2 - k_\parallel^2) \frac{\mathrm{d}\psi}{\mathrm{d}x} \right] - k_y^2 (\Omega^2 - k_\parallel^2 + G) \psi = 0. \tag{23}$$

This dispersion relation yields Alfvén continuous spectra,

$$-k_\parallel - k_y \sigma \leqslant \omega \leqslant -k_\parallel + k_y \sigma, \tag{24}$$

$$k_\parallel - k_y \sigma \leqslant \omega \leqslant k_\parallel + k_y \sigma. \tag{25}$$

We note that this continuum is due to the spatially inhomogeneous Doppler broadening of the Alfvén frequency. This spectrum yields a regular singularity when $\Omega \pm k_\parallel$ is a simple pole, and the corresponding eigenfunction includes logarithmic singularity that is similar to the standard Alfvén waves in an inhomogeneous magnetic field.[11] For $k_\parallel < 2k_y\sigma$, the two Alfvén continua overlap with the flow continuum in the vicinity of $\omega \sim \pm k_\parallel/2$. Moreover, when $k_\parallel < k_y\sigma$, all three continua overlap in the vicinity of $\omega \sim 0$.

In addition to the Alfvén continua (24)–(25), the dispersion relation (23) may produce the point spectra when $G \neq 0$. By multiplying the complex conjugate of flux function ($\overline{\psi}$) on both sides of (23) and integrating it over the domain, we obtain

$$\int_{-1}^{1} (\Omega^2 - k_\parallel^2) \left| \frac{\mathrm{d}\psi}{\mathrm{d}x} \right|^2 \mathrm{d}x + \int_{-1}^{1} k_y^2 (\Omega^2 - k_\parallel^2 + G) \, |\psi|^2 \, \mathrm{d}x = 0. \tag{26}$$

Writing $\omega = \omega_\mathrm{r} + \mathrm{i}\omega_\mathrm{i}$ (ω_r, $\omega_\mathrm{i} \in \mathbb{R}$), the imaginary part of (26) reads

$$\omega_\mathrm{i} \int_{-1}^{1} [\omega_\mathrm{r} - k_y V_y(x)] \left(\left| \frac{\mathrm{d}\psi}{\mathrm{d}x} \right|^2 + k_y^2 |\psi|^2 \right) \mathrm{d}x = 0. \tag{27}$$

We find that the factor $[\omega_r - k_y V_y(x)]$ must change its sign in the domain if unstable ($\omega_\mathrm{i} \neq 0$) solution exists. Then, the corresponding real part ω_r must satisfy

$$-k_y\sigma < \omega_r < k_y\sigma. \tag{28}$$

Once an unstable eigenvalue appears, there are always three others. Suppose ω_e is an eigenvalue of (23) and $\psi_\mathrm{e}(x)$ is the corresponding eigenfunction,

$$\frac{\mathrm{d}}{\mathrm{d}x} \left\{ [(\omega_e - k_y V_y(x))^2 - k_\parallel^2] \frac{\mathrm{d}\psi_e}{\mathrm{d}x} \right\} - k_y^2 [(\omega_e - k_y V_y(x))^2 - k_\parallel^2 + G] \psi_\mathrm{e} = 0. \tag{29}$$

By taking the complex conjugate of both sides, we find that $\overline{\omega_e}$ is also an eigenvalue and $\overline{\psi_e}$ is the corresponding eigenfunction. Since the assumed flow profile (16) satisfies the relation

$$V_y(-x) = -V_y(x), \tag{30}$$

transforming $x = -\tilde{x}$ in (29) yields

$$\frac{\mathrm{d}}{\mathrm{d}\tilde{x}} \left\{ [(\omega_e + k_y V_y(\tilde{x}))^2 - k_\parallel^2] \frac{\mathrm{d}\psi_e(-\tilde{x})}{\mathrm{d}\tilde{x}} \right\} - k_y^2 [(\omega_\mathrm{e} + k_y V_y(\tilde{x}))^2 - k_\parallel^2 + G] \psi_\mathrm{e}(-\tilde{x}) = 0. \tag{31}$$

We thus find that $-\omega_e$ ($-\overline{\omega_e}$) is also an eigenvalue, and that the corresponding eigenfunction is $\psi_e(-x)$ ($\overline{\psi_e}(-x)$).

We end this section by deriving the spectral ODE for the stream function ϕ. For this derivation $k_\parallel$ may be zero [note

that (23) assumes $k_\parallel \neq 0$] but $\Omega = 0$ is not allowed. By solving (18)–(19) with respect to ρ and ψ, respectively, and substituting them into (17), we obtain

$$\frac{d^2\phi}{dx^2} - k_y^2\phi - \frac{2k_y\sigma k_\parallel^2}{\Omega^2(\Omega^2 - k_\parallel^2)}\left(k_y\sigma\phi + \Omega\frac{d\phi}{dx}\right) - \frac{k_y^2 G}{\Omega^2 - k_\parallel^2}\phi = 0. \tag{32}$$

If $V_y'' \neq 0$, an additional term $k_y V_y''\phi/\Omega$ would have appeared on the left-hand side (LHS) of (32) [see (16) of Ref. 12]. In the absence of both the magnetic field ($k_\parallel = 0$) and the interchange drive ($G = 0$), the only source for a possible instability (KH mode) will be this flow curvature term—Rayleigh's inflection point theorem,[8,9] then, shows that V_y'' must change its sign for instability. In the present model ($V_y'' = 0$), however, the complicated denominators and the $d\phi/dx$ term in (32) are the causal of instabilities.

V. PERTURBATIVE ANALYSIS

Here, we will represent a perturbative analysis for the spectral ODE (32) by assuming $\sigma \ll 1$.[13] We expand eigenfunctions and eigenvalues as

$$\phi = \phi_0 + \phi_1 + \phi_2 + \cdots, \quad \omega = \omega_0 + \omega_1 + \omega_2 + \cdots, \tag{33}$$

where $|\omega_h|/|\omega_0| \sim |\phi_h|/|\phi_0| \sim O(\sigma^h)$ for $h \in \mathbb{N}$. Then, the first order correction on the eigenvalue gives $\omega_1 = 0$. To the second order, we obtain (see the Appendix for details)

$$2\omega_0\omega_2 = -\frac{k_\parallel^2\sigma^2}{G}\left(1 + 4P_{4+}B + \frac{16}{\pi^2}P_{4+}^2 A\right) + k_y^2\sigma^2\left(\frac{16}{\pi^6}P_{4+}A + 3B\right), \tag{34}$$

where

$$A = \sum_{m=1}^{\infty} \frac{m^2}{(m^2 - 1/4)^5} \simeq 4.219\,581, \tag{35}$$

$$B = \frac{1}{3} - \frac{2}{\pi^2} \simeq 0.130\,691, \tag{36}$$

$$P_{4+} = k_y^2 + \frac{\pi^2}{4}. \tag{37}$$

For the parameters

$$k_\parallel = k_y = 0.5, \quad G = 2.72, \tag{38}$$

the second order eigenvalue comes out to be

$$\omega_2 = 4.02 i\sigma^2, \tag{39}$$

which shows destabilization due to flow shear (see Fig. 3). The perturbative analysis is applicable as far as $|\omega_2| \ll |\omega_0|$, which translates, in terms of σ, as

$$\sigma \ll 0.0602. \tag{40}$$

On the other hand, $|\phi_1| \ll |\phi_0|$ demands

$$\frac{\sup|\phi_1|}{\sup|\phi_0|} < \sum_{m=1}^{\infty} |q_m| \ll 1 \Leftrightarrow \sigma \ll 0.0764. \tag{41}$$

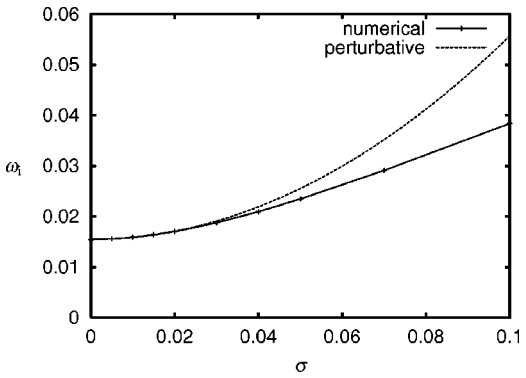

FIG. 3. Comparison of the growth rate between analytic and numerical solutions for the parameter (38). Numerical results are explained in Sec. VII.

When ω_0 describes instability (pure imaginary with $\mathrm{Im}\,\omega_0 > 0$), the first term on the RHS of (34) is destabilizing, while the second is stabilizing. The destabilizing term contains both $k_\parallel$ and G, while the stabilizing one contains only k_y. It is remarkable that $k_\parallel^2$ works to increase the growth rate, and G, decreases it, which is opposite to the conventional understandings for flowless equilibrium. For $k_\parallel = 0$ (or for a neutral fluid), this destabilizing effect does not work. There is a threshold in the ratio of $k_\parallel^2$ and G, where the coefficient of σ^2 changes its sign. The destabilizing condition is

$$\frac{k_\parallel^2}{G} > \frac{k_y^2\left(\frac{16}{\pi^6}P_{4+}A + 3B\right)}{1 + 4P_{4+}B + \frac{16}{\pi^6}P_{4+}^2 A}. \tag{42}$$

Figure 4 shows the threshold as a function of k_y. The threshold of $k_\parallel^2/G$ approaches unity as $k_y \to \infty$. We may conclude, then, that destabilization may occur for any value of $k_\parallel \neq 0$ if k_y is sufficiently small, and for any value of k_y if $k_\parallel^2/G$ is sufficiently large.

VI. VARIATIONAL CALCULATION

The perturbative method is valid only for rather small values of the shear parameter (σ). In this section, therefore, we develop a variational principle approach and explore the effect of larger σ. The spectral ODE for the flux function [see (23)],

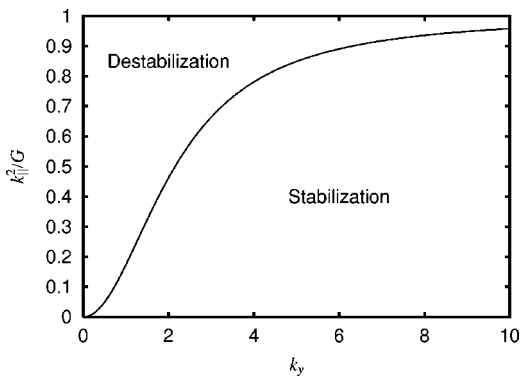

FIG. 4. Parameter regime of flow shear stabilization and destabilization.

$$\frac{\mathrm{d}}{\mathrm{d}x}\left[(\Omega^2-k_\parallel^2)\frac{\mathrm{d}\psi}{\mathrm{d}x}\right]-k_y^2(\Omega^2-k_\parallel^2+G)\psi=0 \tag{43}$$

may be derived by the variation of the Lagrangian,

$$\mathcal{L}=\left\langle(\Omega^2-k_\parallel^2)\left[\left(\frac{\mathrm{d}\psi}{\mathrm{d}x}\right)^2+k_y^2\psi^2\right]\right\rangle+\langle k_y^2G\psi^2\rangle, \tag{44}$$

where the angular bracket denotes the integral covering the domain $[-1,1]$. To find the dispersion relation we may choose a trial function with a variational parameter and find the stationery values of the Lagrangian with respect to the variational parameter. We assume the trial function

$$\psi=\cos\left(\frac{\pi}{2}x\right)+i\alpha\sin(\pi x), \tag{45}$$

where α ($\in\mathbb{R}$) is the unknown parameter to be determined. Note that this trial function is designed as the combination of the most unstable zero-order eigenfunction $\psi_0^{(0)}$ and the dominant first order function $\sin(\pi x)$ derived in the perturbative analysis [see (A3) and (A12)].

Evaluation of $\mathcal{L}$,

$$\mathcal{L}=-P_{1+}(\omega^2+C)\alpha^2-2\mathrm{i}\sqrt{EP_{1+}P_{4+}}\omega\alpha+P_{4+}(\omega^2+D), \tag{46}$$

and imposing $\mathcal{L}=0$ and $\partial_\alpha\mathcal{L}=0$ gives us α and the approximate dispersion relation (after eliminating α)

$$\omega^4+(C+D-E)\omega^2+CD=0, \tag{47}$$

where

$$C=k_y^2\sigma^2\left(\frac{1}{3}-\frac{1}{2\pi^2}\frac{P_{1-}}{P_{1+}}\right)-k_\parallel^2+\frac{k_y^2G}{P_{1+}}, \tag{48}$$

$$D=k_y^2\sigma^2\left(\frac{1}{3}-\frac{2}{\pi^2}\frac{P_{4-}}{P_{4+}}\right)-k_\parallel^2+\frac{k_y^2G}{P_{4+}}, \tag{49}$$

$$E=\frac{64k_y^2\sigma^2}{\pi^4P_{1+}P_{4+}}\left(P_{2+}-\frac{1}{9}P_{2-}\right)^2, \tag{50}$$

$$P_{n\pm}=k_y^2\pm\frac{\pi^2}{n}. \tag{51}$$

In the limit $\sigma\simeq0$, we may neglect E in (47), and then, we have two different solutions,

$$\omega^2+C=0, \quad \text{and} \quad \omega^2+D=0. \tag{52}$$

The branch $\omega^2=-D$ is of interest ($C<D$) to us; with E back in the game, it modifies to

$$\omega^2=-\tfrac{1}{2}(C+D-E)-\tfrac{1}{2}\sqrt{(C+D-E)^2-4CD}. \tag{53}$$

The parameter α is determined by

$$\alpha=-\mathrm{i}\frac{\sqrt{EP_{1+}P_{4+}}\omega}{P_{1+}(\omega^2+C)}, \tag{54}$$

where ω is pure imaginary.

In Fig. 5, we plot the approximate growth rate (53) as a function of the flow shear σ. The growth rate, after an initial monotonic increase, reaches a maximum and then decreases to zero as σ becomes large. Let us estimate the "critical shear parameter" that gives the maximum growth rate. We do it for a relatively small k_y allowing us to omit k_y in $P_{n\pm}$. We also assume that the mode is marginally stable if $\sigma=0$ by taking

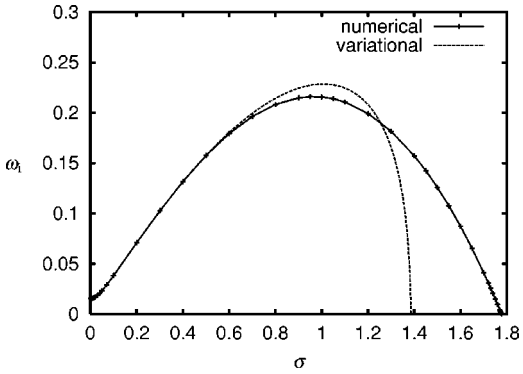

FIG. 5. The growth as a function of the shear parameter σ ($G=2.72$ and $k_y=k_\parallel=0.5$). Numerical results will be derived in Sec. VII.

$$G=\frac{P_{4+}k_\parallel^2}{k_y^2}. \tag{55}$$

Under these conditions we may approximate

$$C+D-E\simeq Qk_y^2\sigma^2+Rk_\parallel^2, \tag{56}$$

$$CD\simeq Sk_y^4\sigma^4+Tk_\parallel^2k_y^2\sigma^2, \tag{57}$$

with numerical coefficients

$$Q\simeq0.109, \quad R\simeq-0.750, \quad S\simeq0.206, \quad T\simeq-0.402. \tag{58}$$

The critical shear will be determined by the condition $\partial_\sigma\omega^2=0$, which translates to

$$-S(Q^2-4S)k_y^4\sigma^4+2S(2T-QR)k_\parallel^2k_y^2\sigma^2+T(T-QR)k_\parallel^4=0, \tag{59}$$

and is solved to find

$$\sigma\simeq\pm1.02\times\frac{k_\parallel}{k_y}. \tag{60}$$

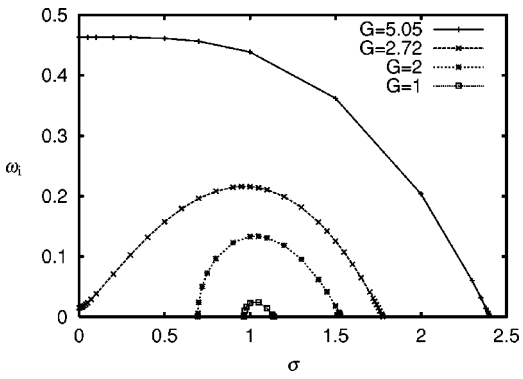

FIG. 6. Flow shear dependence of the growth rate for the parameter $(B_y,B_z)=(1,0)$ and $k_y=k_\parallel=0.5$.

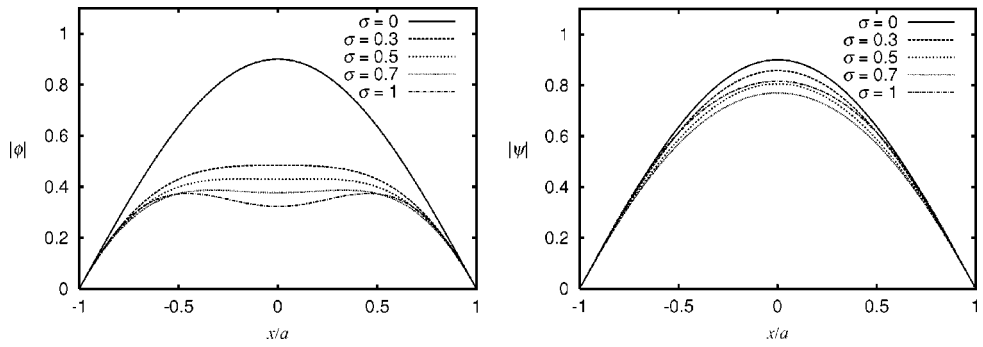

FIG. 7. Mode structures for $G=2.72$ corresponding to Fig. 6.

A direct consequence of (60) is that the local maximum flow velocity $V_{\max}=\sigma$ becomes

$$V_{\max}\sim\frac{k_{\|}v_{\mathrm{A}}}{k_y}=\frac{\omega_{\mathrm{A}}}{k_y}, \tag{61}$$

when the growth rate achieves the maximum value (ω_A is the Alfvén frequency). Beyond this critical velocity (or σ), the growth rate turns to diminish, implying the onset of the stretching effect of the shear flow.

VII. NUMERICAL CALCULATION

In this section, we present results of the numerical analysis of the eigenvalue problem (23) [or equivalently, (32)]. We use a shooting method with fourth order Runge–Kutta formula and a qualified stepper.

In our first example, we take $k_y=k_{\|}=0.5$ for which the system can be unstable for $\sigma=0$. We take $G=2.72$ which is slightly larger than the lower bound (15). In this case, only $n=1$ mode becomes unstable for $\sigma=0$ and its growth rate is estimated by (13) (see Fig. 3),

$$\omega=\pm\,0.0155\mathrm{i}. \tag{62}$$

When we increase the flow shear parameter σ, the growth rate of this mode increases. In order to show the relevance of the analytic calculations, we have superimposed the numerical results on the earlier pictures. In Fig. 3 we see a comparison between the numerical results and previous result from the perturbative analysis. We observe that theoretical growth rates agree well with the numerical ones in the region where the perturbative expansion is applicable [see (40) and (41)]. In Fig. 5 we present a similar comparison of the numerical results with those of the variational approximation, and find that the theory reproduces the general shape of the curve very well; we also find excellent quantitative agreement up to $\sigma\lesssim 1.3$. The comparison is very helpful in showing that the maximum growth rate can be confidently evaluated from the approximate analytic dispersion relation (53).

In Fig. 6, we display the mode growth rate as a function of σ for different values of G. When $G=2.72$, the shear flow enhances the growth rate in the range $\sigma\lesssim 1$ just as was predicted in the previous sections. In this region, the mode structure is bell-shaped and becomes flatter as σ is increased (Fig. 7). Beyond the critical shear ($\sigma\gtrsim 1$), the growth rate diminishes, and the mode undergoes a strong distortion developing symmetric spiky peaks (away from the center; see Fig. 8). When $\sigma\gtrsim 1.78$, the mode is completely stabilized and ''disappears.'' We can also observe in Fig. 6 that there is no shear induced destabilizing for $G\gtrsim 5.04$; the growth rate monotonically decreases with σ. This agrees with the analytical estimate [see (42)]. We further find that even stable modes for $\sigma=0$ ($G=2$ and $G=1$) are destabilized by the Couette flow. In all regions shown in Fig. 6, the eigenvalues are pure imaginary.

Near the upper marginal stability limit of σ, the corresponding mode structure have sharp peaks—the location of peaks depend on G and σ (see Fig. 9). These singularities are related to that of the zero frequency mode $\Omega^2-k_{\|}^2=0$ [flow stretched Alfvén continuum; see (24)–(25)]. For $G=2.72$, 2, and 1, the threshold values are $\sigma\simeq 1.78$, 1.53, and 1.14,

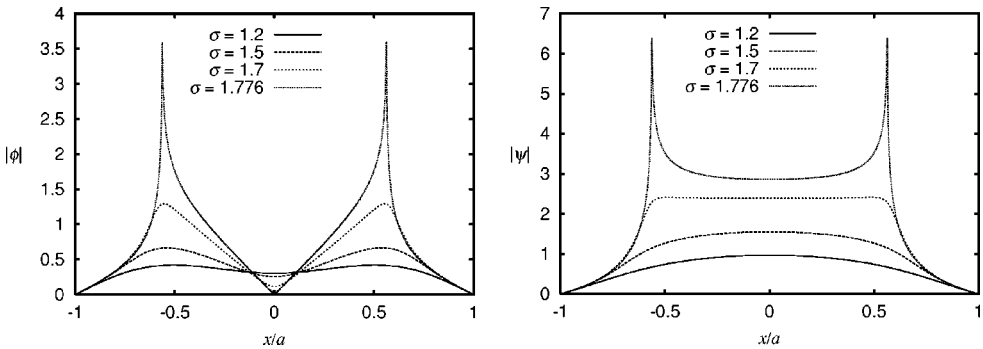

FIG. 8. Mode structures for $G=2.72$ corresponding to Fig. 6.

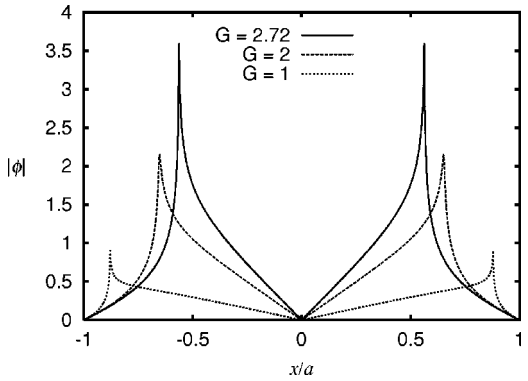

FIG. 9. Upper marginal mode structures.

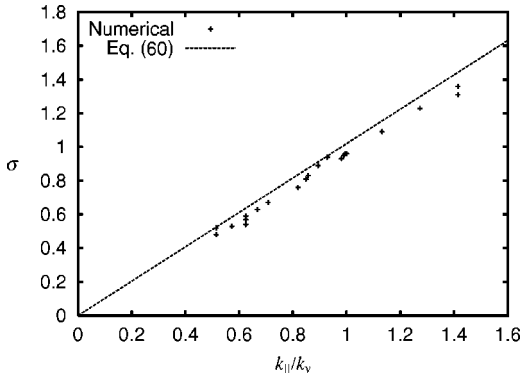

FIG. 11. Maximum growth rate for modes which are almost marginal in case of $\sigma=0$.

respectively. For these values of G and σ, the singular points in the eigenfunctions appear at

$$|x_s| = \frac{k_\parallel}{k_y \sigma} = 0.56, \ \ 0.65, \ \ \text{and} \ \ 0.87, \tag{63}$$

respectively. Since the two Alfvén continua (24)–(25) overlap around $\omega \sim 0$ for $\sigma > 1$, the solution contains multiple singularities. On the other hand, the mode structure near lower marginal stability does not have any singularity, because the Alfvén continua does not extend to $\omega \sim 0$ (see Fig. 10).

For various wave numbers and drives, the maximum growth rate occurs when

$$V_{\max} \simeq \frac{\omega_A}{k_y} \tag{64}$$

is satisfied, if the mode is almost marginally stable for $\sigma = 0$. Numerical results of the survey of maximum growth rate (in the σ-wave number space) are shown in Fig. 11 along with the analytic estimates (60).

Continuing our study of the parametric dependence, we plot the growth rate as a function of G for a fixed σ and $B_z/B_y = 0.1$ (see Fig. 12). We find that $k_\parallel = 0$ mode is stabilized for a higher G than $k_\parallel = 0.5$ mode. We also plot the growth rate as a function of $k_\parallel$ by varying k_z for fixed G, σ, and $k_y = 0.5$ (see Fig. 13). When the flow is absent, the $k_\parallel = 0$ mode is the most unstable (solid line). As we increase σ, however, the dependence of the growth rate on $k_\parallel$ becomes rather weak around $k_\parallel \sim 0$ (dashed line for $G = \sigma = 1$). For a weaker drive (dotted line for $G = 0.8$), we find that $k_\parallel \simeq 0.5$ mode is the most unstable. The maximum growth rate coincides very well with (64). This is due to the fact that the $k_\parallel = 0$ mode will be uniformly stabilized by the flow shear, while nonzero $k_\parallel$ mode is destabilized. Even after the $k_\parallel = 0$ mode is completely stabilized, the mode which satisfies (64) may still remain unstable.

VIII. SUMMARY AND DISCUSSION

We have investigated the effect of the linear shear flow (Couette flow) on interchange type of instabilities. For small flow speeds (compared to the Alfvén velocity), a perturbative analysis shows that the shear flow increases the growth rate of the instability if the parallel wave number is finite. Based on the knowledge of the perturbed eigenfunction, we then derived an approximate dispersion relation valid for arbitrary flow speeds by constructing a variational principle. Approximate dispersion relation shows the growth rate has a maximum with respect to the flow shear. The analytical estimates are found to be in good agreement with numerical solution of the eigenvalue problem.

Shear flows may stabilize instabilities when they stretch the fluctuation. However, we have seen the stabilization occurs only if the local velocity exceeds the phase velocity of the Alfvén wave. When the flow shear is weak to moderate, the modes are generally destabilized; the growth rate

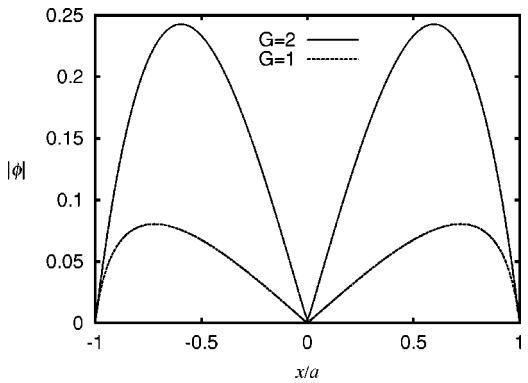

FIG. 10. Lower marginal mode structures.

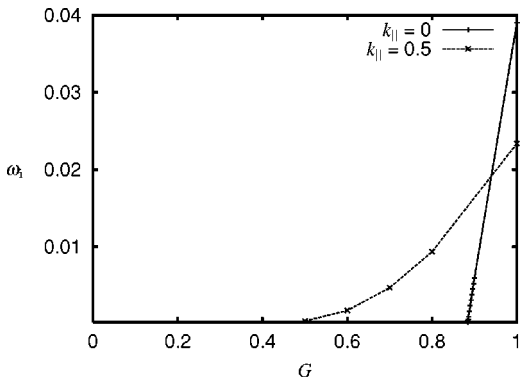

FIG. 12. The G dependence of the growth rate for $\sigma = 1$ and $B_z/B_y = 0.1$.

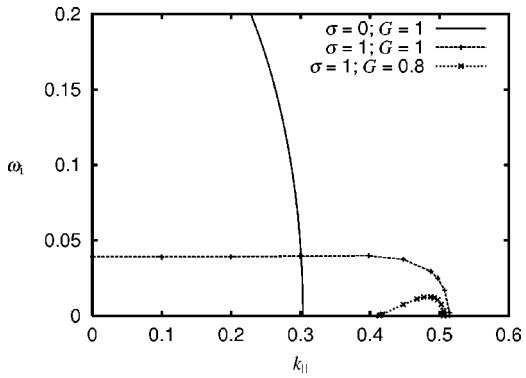

FIG. 13. The $k_\parallel$ dependence of the growth rate for $B_z/B_y=0.1$ and $k_y=0.5$. The zero of $k_\parallel$ corresponds to $k_z=-5$.

achieves its maximum value when the maximum flow velocity is near the Alfvén velocity [see (61)]. For larger flow speeds, the growth rate is suppressed due to the stretching effect which overcomes the Alfvénic phase propagation against the flow. We note that the situation is very different when we consider a mathematical model of infinite-domain linear shear flow. For such a model, the maximum velocity is unbounded, and hence, we see only the stabilization of instabilities.[5]

To understand the destabilization of interchange modes for a weak flow shear let us examine the energy balance in the perturbed fields,

$$\frac{\mathrm{d}}{\mathrm{d}t}\int \frac{1}{2}\rho_0 v^2+\frac{1}{2\mu_0}b^2+\frac{g}{2\rho_0'}\rho_1^2\,\mathrm{d}\mathbf{r} = \int -\rho_0 V_y' v_x v_y+\frac{V_y'}{\mu_0}b_x b_y\,\mathrm{d}\mathbf{r}, \tag{65}$$

where $v^2=v_x^2+v_y^2$ and $b^2=b_x^2+b_y^2$ [see (1)–(3), and below]. In the flowless equilibrium ($V_y=0$), the eigenfunctions determined by (10) are real. Then, we obtain mirror symmetric streamlines which leads to an exact cancellation of the v_xv_y term when integrated. However, an ambient shear flow ($V_y'\neq 0$) yields a complex valued eigenfunction ϕ for which the integral of $v_xv_y$term remains finite because of the breakdown of symmetry. Figure 14 shows the streamlines of the eigenfunction for the cases $\sigma=0.7$ and 1.5 of Fig. 7. We observe that the product v_xv_y is negative in most of the domain if $\sigma=0.7$. Since $V_y'=\sigma$ is a positive constant, this term (representing the work done by the shear flow) gives a positive contribution to the right-hand side of (65). It is remarkable that the stream line contour is inclined in the opposite direction to the ambient shear flow. The mode corresponding to the complex conjugate eigenvalue (damped mode) has the opposite structure—the streamlines are distorted in the direction of the flow. As σ becomes rather large, the ambient flow begins to distort the mode in the direction of flow, and finally stabilizes it.

Our simple model contains only the Alfvén wave, while plasmas are endowed with many other possible waves. How these different waves behave in response to shear flows will make a fascinating study.

ACKNOWLEDGMENTS

The authors are grateful for the fruitful discussions with Professors Wakatani and Hamaguchi of Kyoto University, Professor Carreras of Oak Ridge National Laboratory, and Doctor Ito of the University of Saskatchewan.

One of the authors (T.T.) acknowledges the support from the U.S.–Japan Scientific and Technical Cooperation program, JF1-13. This work was started during his stay in Austin. The work of S.M.M. was supported by the U.S. Department of Energy Contract No. DE-FG03-96ER-54346.

APPENDIX: DETAILS OF PERTURBATIVE ANALYSIS

From the $O(1)$ terms of (32), we obtain

$$\frac{\mathrm{d}^2\phi_0}{\mathrm{d}x^2}-k_y^2\left(1+\frac{G}{\omega_0^2-k_\parallel^2}\right)\phi_0=0, \tag{A1}$$

which has been already solved in Sec. III. Eigenvalues and eigenfunctions are

$$(\omega_0^{(n)})^2=k_\parallel^2-\frac{k_y^2G}{k_y^2+n^2\pi^2/4}, \tag{A2}$$

and

$$\phi_0^{(n)}=\begin{cases}\cos(n\pi x/2) & \text{for } n\text{: odd},\\ \sin(n\pi x/2) & \text{for } n\text{: even},\end{cases} \tag{A3}$$

respectively. We study the effect of the shear flow for the mode $n=1$, that is the most unstable (when $\mathbf{V}_0=\mathbf{0}$).

The terms of $O(\sigma)$ yield

$$\frac{\mathrm{d}^2\phi_1}{\mathrm{d}x^2}-k_y^2\left(1+\frac{G}{\omega_0^2-k_\parallel^2}\right)\phi_1-\frac{2k_yk_\parallel^2\sigma}{\omega_0(\omega_0^2-k_\parallel^2)}\frac{\mathrm{d}\phi_0}{\mathrm{d}x} + \frac{2\omega_0k_y^2G}{(\omega_0^2-k_\parallel^2)^2}(\omega_1-k_y\sigma x)\phi_0=0. \tag{A4}$$

Multiplying $\phi_0^{(1)}$ on both sides of (A4) and integrating it over the domain, we find

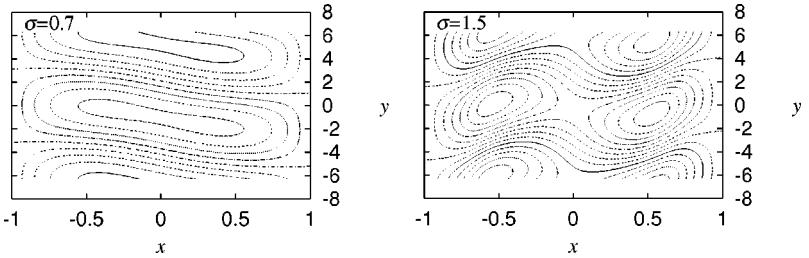

FIG. 14. Streamlines of the typical eigenfunction. The parameters are $B_z=0$, $G=2.72$, $k_\parallel=k_y=0.5$, and $\sigma=0.7$, and 1.5 (see Figs. 6 and 7).

$$\omega_1 = 0. \tag{A5}$$

The next order equation, thus, describes the effect of the flow shear on the eigenvalue. Since the set $\{\phi_0^{(n)}\}$ gives a complete orthogonal basis of the function space, we can expand ϕ_1 as

$$\phi_1 = \sum_{l=1}^{\infty} \{p_l \cos[(l-\tfrac{1}{2})\pi x] + q_l \sin(l\pi x)\}. \tag{A6}$$

Substituting (A6) into (A4) yields, using (A5),

$$\begin{aligned}
&\sum_{l=1}^{\infty} \left\{ -\left(l-\frac{1}{2}\right)^2 \pi^2 p_l \cos\left[\left(l-\frac{1}{2}\right)\pi x\right] - l^2\pi^2 q_l \sin(l\pi x)\right\} \\
&\quad - k_y^2\left(1+\frac{G}{\omega_0^2-k_\parallel^2}\right)\sum_{l=1}^{\infty}\left\{ p_l \cos\left[\left(l-\frac{1}{2}\right)\pi x\right] \right. \\
&\quad \left. + q_l \sin(l\pi x)\right\} + \frac{\pi k_y k_\parallel^2 \sigma}{\omega_0(\omega_0^2-k_\parallel^2)} \sin\left(\frac{\pi}{2}x\right) \\
&\quad - \frac{2k_y\sigma\omega_0 k_y^2 G}{(\omega_0^2-k_\parallel^2)^2} x \cos\left(\frac{\pi}{2}x\right) = 0.
\end{aligned} \tag{A7}$$

Multiplying $\cos(m-1/2)\pi x$ and integrating (A7), we obtain

$$\left[\left(m-\frac{1}{2}\right)^2\pi^2 + k_y^2\left(1+\frac{G}{\omega_0^2-k_\parallel^2}\right)\right] p_m = 0. \tag{A8}$$

We thus find

$$p_m = 0 (\forall m \neq 1). \tag{A9}$$

We note that p_1 does not need to be evaluated, because the corresponding mode is identical to $\phi_0^{(1)}$; we absorb it in the 0-order term and set $p_1 = 0$.

Multiplying $\sin(m\pi x)$ and integrating both sides of (A7) leads to

$$\begin{aligned}
&-\left[m^2\pi^2 + k_y^2\left(1+\frac{G}{\omega_0^2-k_\parallel^2}\right)\right] q_m - \frac{\pi k_y k_\parallel^2\sigma}{\omega_0(\omega_0^2-k_\parallel^2)} \frac{2m(-1)^m}{(m^2-1/4)\pi} \\
&\quad + \frac{2k_y\sigma\omega_0 k_y^2 G}{(\omega_0^2-k_\parallel^2)^2} \frac{2m(-1)^m}{(m^2-1/4)^2\pi^2} = 0,
\end{aligned} \tag{A10}$$

which yields

$$\begin{aligned}
q_m = &\frac{2\sigma}{\pi^2 k_y G\omega_0}\left(k_y^2+\frac{\pi^2}{4}\right)\frac{m(-1)^m}{(m^2-1/4)^2} \\
&\times\left[k_\parallel^2 + \left(k_y^2+\frac{\pi^2}{4}\right)\frac{2\omega_0^2}{(m^2-1/4)\pi^2}\right].
\end{aligned} \tag{A11}$$

The first-order correction to the eigenfunction is

$$\phi_1 = \sum_{m=1}^{\infty} q_m \sin(m\pi x). \tag{A12}$$

Since ω_0 is a pure imaginary (supposed to be unstable; see Sec. II), the first-order correction (due to a flow) adds an odd pure imaginary function ϕ_1 on a real and even zero-order eigenfunction.

The next order ODE is

$$\begin{aligned}
&\frac{d^2\phi_2}{dx^2} - k_y^2\left(1+\frac{G}{\omega_0^2-k_\parallel^2}\right)\phi_2 - \frac{2k_y k_\parallel^2\sigma}{\omega_0(\omega_0^2-k_\parallel^2)}\frac{d\phi_1}{dx} \\
&\quad - \frac{2\omega_0 k_y^3 G\sigma}{(\omega_0^2-k_\parallel^2)^2} x\phi_1 - \frac{2k_y^2k_\parallel^2(3\omega_0^2-k_\parallel^2)\sigma^2}{\omega_0^2(\omega_0^2-k_\parallel^2)^2} x\frac{d\phi_0}{dx} \\
&\quad - \frac{k_y^4 G(3\omega_0^2+k_\parallel^2)\sigma^2}{(\omega_0^2-k_\parallel^2)^3} x^2\phi_0 \\
&\quad + \left[\frac{2k_y^2 G\omega_0}{(\omega_0^2-k_\parallel^2)^2}\omega_2 - \frac{2k_y^2k_\parallel^2\sigma^2}{\omega_0^2(\omega_0^2-k_\parallel^2)}\right]\phi_0 = 0,
\end{aligned} \tag{A13}$$

which may be used to estimate ω_2. Making the quadratic form, we obtain

$$\begin{aligned}
&\frac{2k_y k_\parallel^2\sigma}{\omega_0}\sum_{m=1}^{\infty}\frac{m\,(-1)^m}{m^2-1/4} q_m \\
&\quad + \frac{2\omega_0 k_y^3 G\sigma}{\omega_0^2-k_\parallel^2}\sum_{m=1}^{\infty}\frac{2m\,(-1)^m}{(m^2-1/4)^2\pi^2} q_m \\
&\quad + \frac{k_y^2k_\parallel^2(3\omega_0^2-k_\parallel^2)\sigma^2}{\omega_0^2(\omega_0^2-k_\parallel^2)} - \frac{k_y^4 G(3\omega_0^2+k_\parallel^2)\sigma^2}{(\omega_0^2-k_\parallel^2)^2}\left(\frac{1}{3}-\frac{2}{\pi^2}\right) \\
&\quad + \frac{2k_y^2 G\omega_0}{\omega_0^2-k_\parallel^2}\omega_2 - \frac{2k_y^2k_\parallel^2\sigma^2}{\omega_0^2} = 0.
\end{aligned} \tag{A14}$$

Using[15]

$$\sum_{m=1}^{\infty}\frac{m^2}{(m^2-1/4)^3} = \frac{\pi^2}{4}, \tag{A15}$$

we finally obtain the second order dispersion relation (34).

[1] H. Helmholtz, Philos. Mag. **36**, 337 (1868); W. Thomson (Lord Kelvin), *ibid.* **42**, 362 (1871).
[2] M. E. Stern, Phys. Fluids **6**, 636 (1959); A. Kent, J. Plasma Phys. **2**, 543 (1968); X. L. Chen and P. J. Morrison, Phys. Fluids B **3**, 863 (1991).
[3] E. Frieman and M. Rotenberg, Rev. Mod. Phys. **32**, 898 (1960).
[4] A. Bondeson, R. Iacono, and A. Battacharjee, Phys. Fluids **30**, 2167 (1987).
[5] T. Tatsuno, F. Volponi, and Z. Yoshida, Phys. Plasmas **8**, 399 (2001).
[6] M. Hirota, T. Tatsuno, S. Kondoh, and Z. Yoshida, Phys. Plasmas **9**, 1177 (2002).
[7] H. R. Strauss, Phys. Fluids **20**, 1354 (1977).
[8] J. W. S. Rayleigh, Proc. London Math. Soc. **9**, 57 (1880).
[9] P. G. Drazin and W. H. Reid, *Hydrodynamic Stability* (Cambridge University Press, Cambridge, 1981).
[10] J. P. Goedbloed and P. H. Sakanaka, Phys. Fluids **17**, 908 (1974).
[11] J. A. Tataronis and W. Grossmann, Z. Phys. **261**, 203 (1973).
[12] A. Ito, Z. Yoshida, T. Tatsuno, S. Ohsaki, and S. M. Mahajan, Phys. Plasmas **9**, 4856 (2002).
[13] S. Hamaguchi and W. Horton, Phys. Fluids B **4**, 319 (1992).
[14] S. Chandrasekhar, *Hydrodynamic and Hydromagnetic Stability* (Clarendon, Oxford, 1961).
[15] I. S. Gradshteyn and I. M. Ryzhik, *Table of Integrals, Series, and Products* (Academic, New York, 1994).